Mathematical modelling and computer simulation of the flow around a Formula 1 racing car

[1]T. A. CHRYSOLORAS, [1,2]N.C. MARKATOS*

[1]Computational Fluid Dynamics Unit, School of Chemical Engineering
National Technical University of Athens
Iroon Polytechniou 9, GR-15780, GREECE

[2]School of Chemical Engineering, National Technical University of Athens, Iroon Polytechniou 9, GR-15780 GREECE.

Abstract: Automobile racing is an extremely popular sport worldwide, with its beginning dating back to the 19th century. Since that era, the evolution of this sector of activity has been continuous. As a result, the sport, as it is known nowadays, has very little to do with its early form. Automobile racing, apart from being a pleasant spectacle for the fans of the sport, also comprises a deeper and more essential role. It is a sector, in which automotive industries are in a constant battle, by trying novel technologies and examining the way these technologies affect the behavior of the vehicles on the track and their ability to offer them victories, against their rivals. These technologies mainly concern the technical specifications of the vehicles, such as the engine's horsepower, the aerodynamic traits, or even the tires' dimensions and the chassis characteristics. Although, according to popular opinion, the human factor has a prominent role in the success (or failure) in the particular sport, no one can deny the fact that the technological advances often have an equally – if not more – important role. In the present work, the effect of some geometrical characteristics of a Formula 1 vehicle on the drag force and on the down force, exerted on it – and, consequently, on the drag and lift coefficient values –, is studied. The geometrical characteristics studied here refer to the ride's height and the wheels' diameter and the study is conducted using various turbulence models of increasing complexity, which is actually its originality. Comparing the results obtained, the work concludes proposing what one expects to obtain using this approach and which turbulence model yields the best agreement with experimental data and, therefore, it is recommended for practical design.

Keywords: aerodynamics; turbulence; drag coefficient; lift coefficient; PHOENICS

Received: May 14, 2021. Revised: January 17, 2022. Accepted: February 21, 2022. Published: April 4, 2022.

1. Introduction

The purpose of the work described in the present paper is the aerodynamic study around a motorsports vehicle and more specifically around a racing car of the Formula 1 sport.

One of the most important – if not the most important – factor in this sport is the aerodynamic behavior of the vehicle which is associated with the forces that act upon it. The main forces exerted on a moving vehicle, can be seen in *Figure 1*.

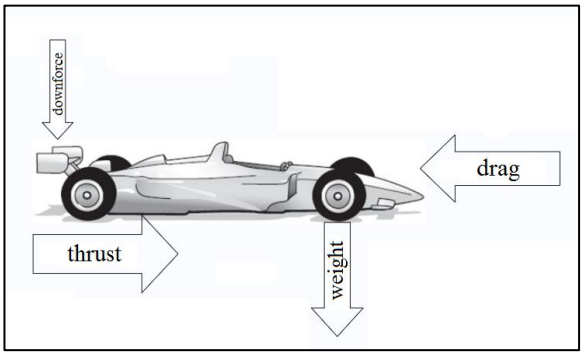

Figure 1: Depiction of the main forces, which are exerted on a moving vehicle.

The drag force opposes the vehicle's motion through the air and tends to reduce its speed. Down force is related to the vertical pressure on the car's body and may change, depending on its aerodynamic characteristics. Thrust is the force generated by the vehicle's engine, while weight results from the gravitational attraction of the Earth on it. The primary goal set by car manufacturers, in all circumstances, is the reduction of drag. Apart from that, the increase of downforce is often desired, so that the car has better cornering ability. Drag force affects the way in which the vehicle passes through the surrounding air, while downforce is the force which allows it to turn more safely, even at high speeds. The two quantities, which are associated with drag and downforce are the drag and lift coefficients, respectively (symbolized as C_d and C_l). It is preferable that those quantities have the lowest possible value, so that the vehicles can be driven both fast and safely.

The work reported here is the study of the effect of the aerodynamic characteristics of a Formula 1 car on those two coefficients. Namely, the ride's height and the wheels' diameter are altered, and the effect of these alterations on the drag and lift coefficients is studied.

2. The problem considered

2.1. Geometry

To conduct the necessary calculations, the software PHOENICS v1.0 was used, appropriately modified. The examined test case regards a reduced model Jaguar Formula 1 racing car. The problem's geometry is displayed in *Figure 2*.

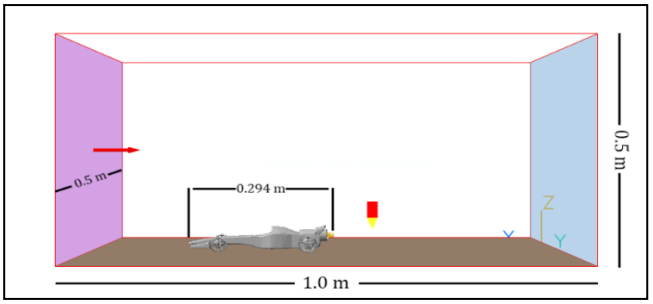

Figure 2: Depiction of the geometry of the model car considered. The model's dimensions can also be seen in Table 1 (see Section 3.1).

This case was used for all studies carried out, with the necessary modifications, such as the change of the turbulence model used, the grid's dimensions and the vehicle's aerodynamic traits. The changes were made in such a way, always to be in accordance with Formula 1 regulations.

2.2. Mathematical modelling

2.2.1. Assumptions

For the mathematical modelling the following assumptions were made:

- No heat transfer between the vehicle and the environment.
- Constant air inlet velocity into the computational domain.
- The model car considered was assumed to be in a wind tunnel, therefore the computational domain boundaries (apart from inlet/outlet) were considered as walls, with no slip condition.
- Incompressible flow; therefore, Mach number with a value lower than 0.3 [1]. The above assumptions are not restrictions of the present model, which is general, but were considered reasonable for the sake of computational economy.

2.2.2. Governing Differential Equations

The equations describing the problem are the continuity and the Navier – Stokes equations, listed below [2, 3].

Continuity Equation

$$\frac{\partial \rho}{\partial t} + \frac{\partial (\rho u)}{\partial x} + \frac{\partial (\rho v)}{\partial y} + \frac{\partial (\rho w)}{\partial z} = 0 \quad (2.1)$$

Navier – Stokes Equations

$$\frac{\partial (\rho u)}{\partial t} + \nabla \cdot (\rho u \vec{\boldsymbol{u}}) = -\frac{\partial p}{\partial x} + \frac{\partial \sigma_{xx}}{\partial x} + \frac{\partial \sigma_{xy}}{\partial y} + \frac{\partial \sigma_{xz}}{\partial z} + F_x \quad (2.2)$$

$$\frac{\partial (\rho v)}{\partial t} + \nabla \cdot (\rho v \vec{\boldsymbol{u}}) = -\frac{\partial p}{\partial y} + \frac{\partial \sigma_{yx}}{\partial x} + \frac{\partial \sigma_{yy}}{\partial y} + \frac{\partial \sigma_{yz}}{\partial z} + F_y \quad (2.3)$$

$$\frac{\partial (\rho w)}{\partial t} + \nabla \cdot (\rho w \vec{\boldsymbol{u}}) = -\frac{\partial p}{\partial z} + \frac{\partial \sigma_{zx}}{\partial x} + \frac{\partial \sigma_{zy}}{\partial y} + \frac{\partial \sigma_{zz}}{\partial z} + F_z \quad (2.4)$$

Where u, v and w are the velocity components, ρ is the density, σ_{ij} are the components of the stress tensor and F_i is the i – component of the body forces.

3. Numerical solution

3.1. Vehicle dimensions and computational domain characteristics

As already mentioned, the base case used concerns a model Jaguar Formula 1 racing car. The model's dimensions are shown in *Table 1*. This model is a scaled representation of a real racing car.

Table 1: The model's default dimensions (expressed in meters).

Ride height	Front wheel diameter	Rear wheel diameter	Length	Width	Height
0.005	0.035	0.040	0.294	0.042	0.054

The computational domain used for the calculations, was a rectangular parallelepiped, with length of 1.0-meter, width of 0.5 meters and height of 0.5 meters ($1.0x0.5x0.5$), while the air inlet velocity was considered equal to 18 m/s.

3.2. Turbulence models used

For the calculations, three different advanced turbulence models were used and their results were compared. Those turbulence models were the:

1. k – ω SST turbulence model
2. LES – Smagorinsky turbulence model
3. Reynolds- Stress Transport Model (RSTM)

3.2.1. k – ω SST turbulence model

The k – ω turbulence model is widely used in Computational Fluid Dynamics (CFD). It makes use of two transport equations, the first being that for the turbulence kinetic energy, k, while the second regards the specific dissipation rate of the turbulence kinetic energy, ω.

Generally, the k – ω turbulence model allows a more precise analysis, than the k-ε model, of the flow in the areas which are located close to solid walls and is highly efficient in cases of flows with a low Reynolds number. Furthermore, it yields reliable results, in cases of flow separation from smooth surfaces, in contrast with the k – ε turbulence model, which overestimates the time required, for the separation to be initiated.

There are two main variations of the k – ω turbulence model:

- Wilcox k – ω turbulence model [4, 5, 6].
- Menter k – ω SST (Shear Stress Transport) turbulence model [4, 7, 8].

The k – ω SST turbulence model was introduced by Menter, in 1994 and it was chosen for the present study. The main purpose of this model is to overcome the insufficiencies of the k – ε and k – ω turbulence models, by combining both. More specifically, this turbulence model is aimed at improving the prediction of the adverse pressure – gradient cases [4] and dealing with the problems, due to the strong sensitivity of the original k – ω turbulence model, of the free stream flow. Thus, the k – ω SST turbulence model renders possible the usage of the k – ε turbulence model in areas of free shear flow, and the usage of the k – ω turbulence model in the inner region of the boundary layer [4].

The main equations of the k – ω SST turbulence model, are listed below [9]:

$$\frac{\partial(\rho k)}{\partial t}+\frac{\partial\left(\rho k u_j\right)}{\partial x_j}=\tau_{ij}\frac{\partial u_i}{\partial x_j}-\beta^*\rho k\omega+\frac{\partial}{\partial x_j}\left[(\mu+\sigma_k\mu_t)\frac{\partial k}{\partial x_j}\right] \quad (3.1)$$

$$\frac{\partial(\rho\omega)}{\partial t}+\frac{\partial\left(\rho\omega u_j\right)}{\partial x_j}=\frac{\rho\gamma}{\mu_t}\tau_{ij}\frac{\partial u_i}{\partial x_j}-\beta\rho\omega^2+\frac{\partial}{\partial x_j}\left[(\mu+\sigma_\omega\mu_t)\frac{\partial\omega}{\partial x_j}\right]+2(1-F_1)\frac{\rho\sigma_{\omega2}}{\omega}\frac{\partial k}{\partial x_j}\frac{\partial\omega}{\partial x_j} \quad (3.2)$$

Where μ_t is the turbulence eddy viscosity, which, in this case, is calculated as:

$$\mu_t=\frac{\rho\alpha_1 k}{\max(\alpha_1\omega,\Omega F_2)} \quad (3.3)$$

The blending functions F_1 and F_2 are calculated as follows:

$$F_1=\tanh(arg_1^4) \quad (3.4)$$

$$F_2=\tanh(arg_2^4) \quad (3.5)$$

Where:

$$arg_1 = min\left[max\left(\frac{\sqrt{k}}{\beta^* \omega d}, \frac{500v}{\omega d^2}\right), \frac{4\rho\sigma_{\omega 2} k}{d^2 CD_{k\omega}}\right] \quad (3.6)$$

$$arg_2 = max\left(2\frac{\sqrt{k}}{\beta^* \omega d}, \frac{500v}{\omega d^2}\right) \quad (3.7)$$

$$CD_{k\omega} = \max\left(2\rho\sigma_{\omega 2}\frac{1}{\omega}\frac{\partial k}{\partial x_j}\frac{\partial \omega}{\partial x_j}, 10^{-20}\right) \quad (3.8)$$

$$\Omega = \sqrt{2W_{ij}W_{ij}}, with\ W_{ij} = \frac{1}{2}\left(\frac{\partial u_i}{\partial x_j} - \frac{\partial u_j}{\partial x_i}\right) \quad (3.9)$$

In Equations (3.6) and (3.7), d is the distance from the solid wall.

Finally, the values of the model constants are the following:

k – ω closure

$$\gamma_1 = \frac{\beta_1}{\beta^*} - \frac{\sigma_{\omega 1}\kappa^2}{\sqrt{\beta^*}} \quad \sigma_{k1} = 0.85 \quad \sigma_{\omega 1} = 0.5 \quad \beta_1 = 0.075 \quad (3.10)$$

k – ε closure

$$\gamma_2 = \frac{\beta_2}{\beta^*} - \frac{\sigma_{\omega 2}\kappa^2}{\sqrt{\beta^*}} \quad \sigma_{k2} = 1.00 \quad \sigma_{\omega 2} = 0.856 \quad \beta_2 = 0.0828 \quad (3.11)$$

SST closure

$$a_1 = 0.31 \qquad \beta^* = 0.09 \qquad \kappa = 0.41 \quad (3.12)$$

3.2.2. LES – Smagorinsky LES turbulence model

Large Eddy Simulation (LES) is a mathematical model for turbulence initially proposed in 1963, by Joseph Smagorinsky, in order to simulate atmospheric air currents and first explored by Deardorff. In modern times, LES is used in a wide variety of engineering applications, including combustion, acoustics, as well as simulations of the atmospheric boundary layer.

In Large Eddy Simulations of turbulent flows, subgrid – scale (SGS) turbulence models are used. The LES approach is, essentially, a combination of Direct Numerical Simulation (DNS) of turbulence and conventional

turbulence modelling. The large scales of turbulence (eddies) are simulated directly, while the small (sub – grid) scales are modelled with a SGS turbulence model. In this way, the flow variables are decomposed in terms of:

- resolved (grid) scales
- unresolved (sub – grid) scales,

rather than time – mean and fluctuating quantities.

The averaging operation results in the appearance of unknown SGS stresses, which are modeled by making use of a SGS turbulence model. The simplest and most widespread SGS turbulence model used is the Smagorinsky turbulence model.

In the LES – Smagorinsky turbulence model, the elements of the deviatoric stress tensor are modelled as [4]:

$$\tau_{ij} - \frac{1}{3}\tau_{kk}\delta_{ij} = -2\frac{\mu_t}{\rho}S_{ij} \qquad (3.13)$$

Where τ_{ij} and τ_{kk} regard the elements of the residual stress tensor, δ_{ij} is the Kronecker delta, μ_t is the turbulence eddy viscosity, ρ is the density and the quantity S_{ij} represents the rate – of – strain tensor, the elements of which are equal to:

$$S_{ij} = \frac{1}{2}\left(\frac{\partial u_i}{\partial x_j} + \frac{\partial u_j}{\partial x_i}\right) \qquad (3.14)$$

Where x_i and x_j represent the elements of the coordinate vector, while u_i and u_j represent the elements of the velocity field.

The turbulence eddy viscosity is calculated as follows:

$$\mu_t = \rho(C_s\Delta)^2|\bar{S}| \qquad (3.15)$$

Where Δ is a representative mesh interval, which is defined as:

$$\Delta = (V_{cell})^{\frac{1}{3}} \qquad (3.16)$$

V_{cell} is the volume of the computational cell.

The quantity $|\bar{S}|$ is equal to:

$$|\bar{S}| = \sqrt{S_{ij}S_{ij}} \qquad (3.17)$$

Finally, C_s is the Smagorinsky's constant, the value of which varies with application and ranges from 0.1 to 0.25. The constant's value, which is used in this study is equal to 0.17, a value suggested from previous experience as statistically best.

3.2.3. Reynolds Stress Transport Model (RSTM)

The Reynolds-Stress Model (RSM) is a higher level RANS turbulence model, using a second-order closure, and represents the most reliable of the classical models. It originates from the works by Chou (1945) and Rotta (1951), and it avoids the eddy – viscosity hypothesis, computing directly all six components of the Reynolds stress tensor. The RSM is able to account for complex interactions in turbulent flow fields, such as the directional effects of the Reynolds stresses [4].

The RSM involves the solution of seven transport equations (3 for the normal stresses, 3 for the shearing stresses and the equation for the dissipation rate, ε).

The Reynolds stress transport equations may be written in the following symbolic tensor form:

$$T_{ij} + C_{ij} = D_{ij} + P_{ij} + R_{ij} - E_{ij} \qquad (3.18)$$

Where T_{ij} is the transient term, C_{ij} is the convection term, D_{ij} is the diffusion term, P_{ij} is

the production term, R_{ij} is the redistribution term and E_{ij} is the dissipation term. The redistribution term, R_{ij}, is the most important term requiring closure and it is commonly known as the pressure – strain term.

4. Grid- independency study

A detailed grid-independency study was carried out and sample results are presented here.

- The computational grids used were: $60x42x30$, $105x62x60$, $145x82x75$, $165x95x85$ and $175x100x90$.

The grid- independency study took place for all three turbulence models, and for the following two cases:

- A ride height of 0.020 m, front wheel diameter of 0.035 m and rear wheel diameter of 0.040 m.
- A ride height of 0.005 m, front wheel diameter of 0.030 m and rear wheel diameter of 0.040 m.

Sample results obtained can be seen in *Tables 2* to *7*.

Table 2: Overall grid -independency study results, for the first case (k – ω SST turbulence model).

Computational Grid	Drag Coefficient (C_d)	Lift Coefficient (C_l)
Grid #1 $(60x42x30)$	0.610	0.077
Grid #2 $(105x62x60)$	0.741	0.024
Grid #3 $(145x82x75)$	0.728	0.033
Grid #4 $(165x95x85)$	0.715	0.017
Grid #5 $(175x100x90)$	0.718	0.017

Table 3: Overall grid -independency study results, for the first case (LES – Smagorinsky turbulence model).

Computational Grid	Drag Coefficient (C_d)	Lift Coefficient (C_l)
Grid #1 $(60x42x30)$	0.623	0.092
Grid #2 $(105x62x60)$	0.754	0.037
Grid #3 $(145x82x75)$	0.745	0.029
Grid #4 $(165x95x85)$	0.726	0.022
Grid #5 $(175x100x90)$	0.725	0.021

Table 4: Overall grid -independency study results, for the first case (RSTM).

Computational Grid	Drag Coefficient (C_d)	Lift Coefficient (C_l)
Grid #1 ($60x42x30$)	0.608	0.063
Grid #2 ($105x62x60$)	0.739	0.027
Grid #3 ($145x82x75$)	0.731	0.016
Grid #4 ($165x95x85$)	0.711	0.010
Grid #5 ($175x100x90$)	0.708	0.010

Table 5: Overall grid -independency study results, for the second case (k – ω SST turbulence model).

Computational Grid	Drag Coefficient (C_d)	Lift Coefficient (C_l)
Grid #1 ($60x42x30$)	0.616	0.094
Grid #2 ($105x62x60$)	0.682	0.080
Grid #3 ($145x82x75$)	0.674	0.037
Grid #4 ($165x95x85$)	0.691	0.019
Grid #5 ($175x100x90$)	0.688	0.018

Table 6: Overall grid -independency study results, for the second case (LES - Smagorinsky turbulence model).

Computational Grid	Drag Coefficient (C_d)	Lift Coefficient (C_l)
Grid #1 ($60x42x30$)	0.627	0.089
Grid #2 ($105x62x60$)	0.679	0.075
Grid #3 ($145x82x75$)	0.695	0.035
Grid #4 ($165x95x85$)	0.699	0.016
Grid #5 ($175x100x90$)	0.702	0.016

Table 7: Overall grid- independency study results, for the second case (RSTM).

Computational Grid	Drag Coefficient (C_d)	Lift Coefficient (C_l)
Grid #1 ($60x42x30$)	0.615	0.076
Grid #2 ($105x62x60$)	0.667	0.072
Grid #3 ($145x82x75$)	0.680	0.029
Grid #4 ($165x95x85$)	0.689	0.014
Grid #5 ($175x100x90$)	0.684	0.015

By examining the evolution of the drag and lift coefficient values, but also the excessive results on velocity and pressure distributions that are not presented here because of space limitations, it becomes clear that, for the two last computational grids, grid independence has essentially been achieved, since the values, either remain invariable, or display a slight alteration, the magnitude of which, in all circumstances, is lower than (or, at least, approximately equal to) 5%. This level of precision has been considered as adequate for the present study, since further grid refinement would entail a significant increase in computational cost and, thus, be uneconomical. Therefore, the optimal computational grid for the present study, is the one of dimensions $165x95x85$.

The variation of the drag and lift coefficients with the computational grids can be seen in *Figures 3* to *6*.

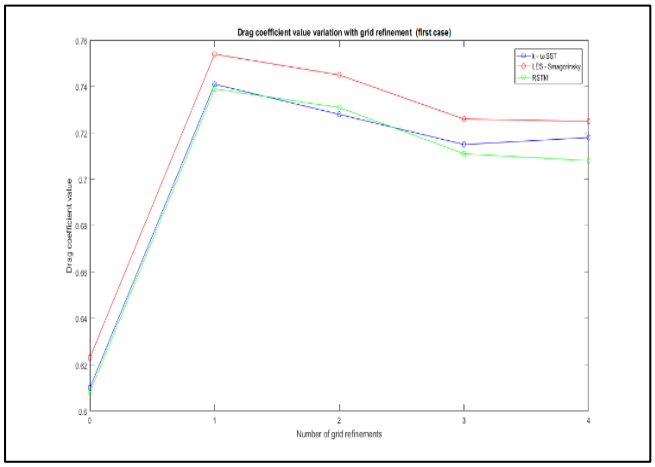

Figure 3: Variation of the drag coefficient, with the computational grid's refinement, for the three turbulence models used (first case).

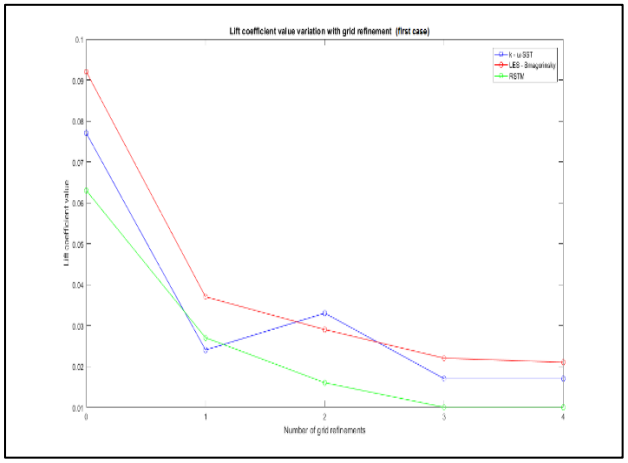

Figure 4: Variation of the lift coefficient, with the computational grid's refinement, for the three turbulence models used (first case).

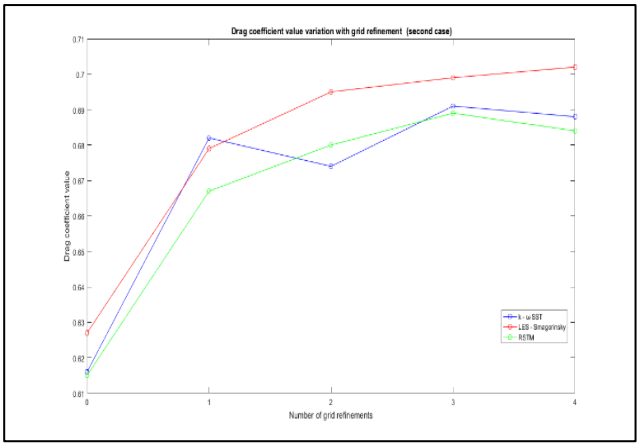

Figure 5: Variation of the drag coefficient, with the computational grid's refinement, for the three turbulence models used (second case).

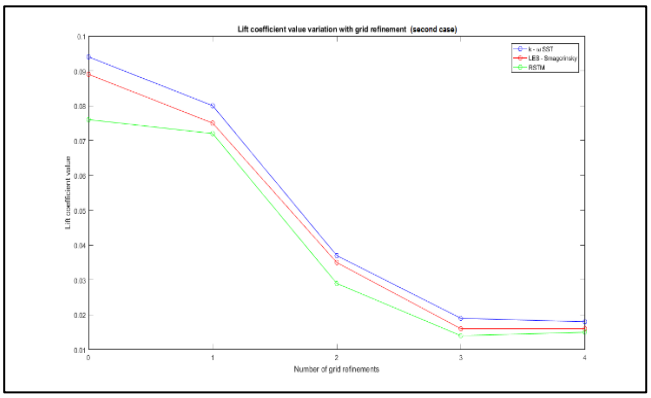

Figure 6: Variation of the lift coefficient, with the computational grid's refinement, for the three turbulence models used (second case).

As it can be seen from *Figures 3* to *6*, the values of the aerodynamic coefficients calculated using the RSTM are lower than the ones calculated by the other two turbulence models, for the optimal computational grid. This demonstrates the importance of grid independence of results, as for the coarser grids the aerodynamic coefficients calculated by the k – ω SST turbulence model have a lower value than the ones calculated by the RSTM and may lead to wrong conclusions.

5. Case studies

5.1. Study of the ride height's effect

In the first case, the effect of the ride height's variation on the flow development around the car and on the drag and lift coefficients was studied, for the three turbulence models used.

5.1.1. Geometrical characteristics

The racing car's geometrical characteristics, for the three different cases that were studied for the ride height, are listed in *Table 8*. As it is clearly seen, a gradual increase in the ride height was made, initially from 0.005 m to 0.010 m and then to 0.020 m.

Table 8: The model's dimensions, which were used in the three examined cases (expressed in meters).

Case	Ride height	Front wheel diameter	Rear wheel diameter	Length	Width	Height
1	0.005	0.035	0.040	0.294	0.042	0.054
2	0.010	0.035	0.040	0.294	0.042	0.054
3	0.020	0.035	0.040	0.294	0.042	0.054

Each of the three aforementioned cases was studied, by using all three turbulence models mentioned in **Section 3.2**. Therefore, a total of nine sets of calculations were conducted.

5.1.2. Results and observations

The predicted drag and lift coefficients are shown in *Table 9*.

Table 9: Effect of the ride's height on the calculated drag and lift coefficients, for the three turbulence models.

Case	Turbulence Model	Ride height (m)	Drag Coefficient (C_d)	Lift Coefficient (C_l)
1.1	k – ω SST	0.005	0.653	0.099
1.2	k – ω SST	0.010	0.631	0.106
1.3	k – ω SST	0.020	0.610	0.077
2.1	LES – Smagorinsky	0.005	0.667	0.094
2.2	LES – Smagorinsky	0.010	0.629	0.100
2.3	LES – Smagorinsky	0.020	0.623	0.092
3.1	RSTM	0.005	0.661	0.080
3.2	RSTM	0.010	0.628	0.108
3.3	RSTM	0.020	0.608	0.063

From the results of *Table 9*, it is observed that the drag coefficient decreases, as the ride's height increases. On the contrary, the lift coefficient initially rises and then it decreases, reaching a lower value than the one calculated for a ride height of 0.005 m (marginally lower, for the LES – Smagorinsky turbulence model). This tendency is observed for all three turbulence models used.

It is additionally concluded that, for a ride height value of 0.020 m, both the drag and lift coefficient reach their minimum value. In fact, the values that the Reynolds stress transport model yields are the lowest in the specific case. In particular, the drag and lift coefficient values are **0.3279%** and **18.18%** lower, respectively, than the ones predicted by the k – ω SST turbulence model, and **2.408%** and **31.52%** lower, respectively, than the ones obtained by the LES – Smagorinsky turbulence model.

Figures 7 to 24 present pressure and velocity contours, as viewed in the xz-plane, for the three different ride heights and the three different turbulence models.

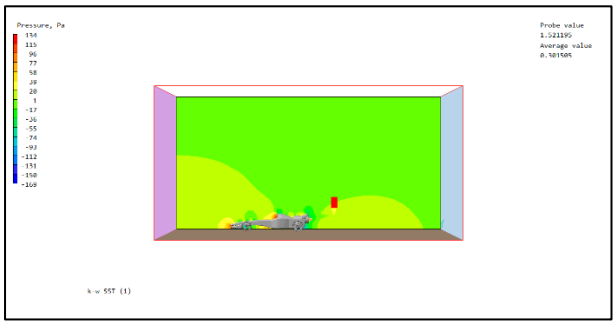

Figure 7: Depiction of the pressure contours, for a ride height of 0.005 m (xz – plane, k – ω SST turbulence model).

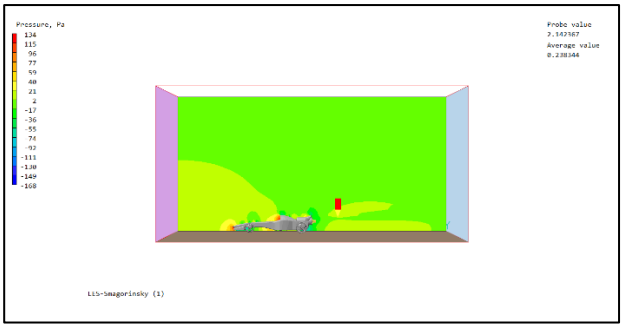

Figure 8: Depiction of the pressure contours, for a ride height of 0.005 m (xz – plane, LES – Smagorinsky turbulence model).

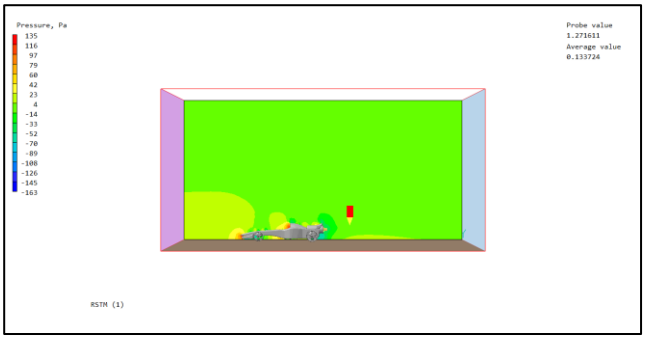

Figure 9: Depiction of the pressure contours, for a ride height of 0.005 m (xz – plane, RSTM).

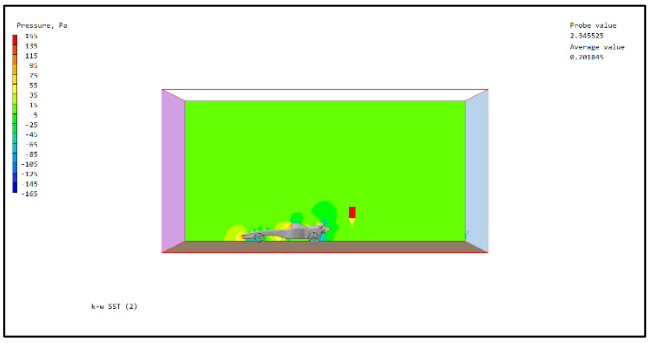

Figure 10: Depiction of the pressure contours, for a ride height of 0.010 m (xz – plane, k – ω SST turbulence model).

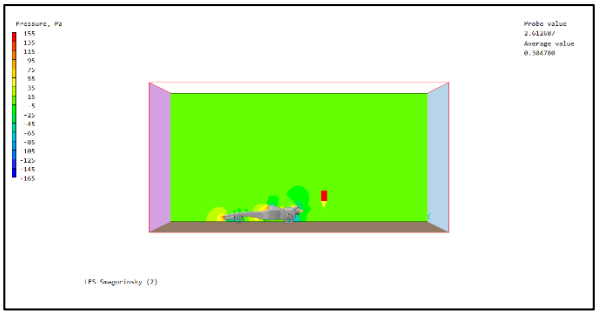

Figure 11: Depiction of the pressure contours, for a ride height of 0.010 m (xz – plane, LES – Smagorinsky turbulence model).

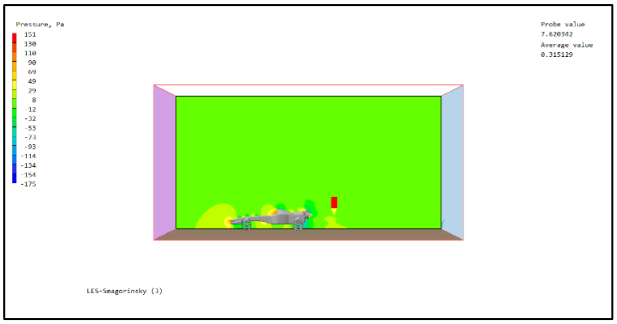

Figure 14: Depiction of the pressure contours, for a ride height of 0.020 m (xz – plane, LES – Smagorinsky turbulence model).

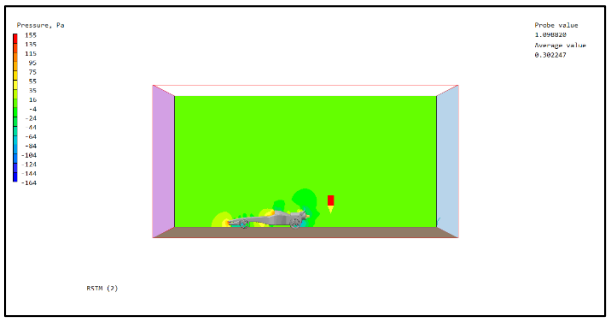

Figure 12: Depiction of the pressure contours, for a ride height of 0.010 m (xz – plane, RSTM).

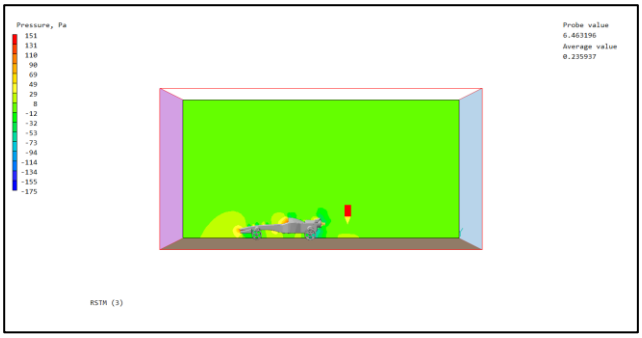

Figure 15: Depiction of the pressure contours, for a ride height of 0.020 m (xz – plane, RSTM).

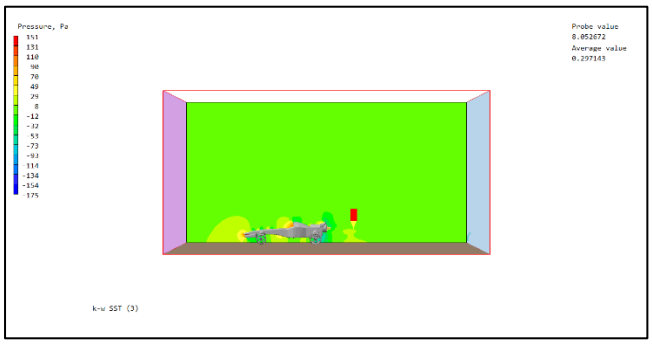

Figure 13: Depiction of the pressure contours, for a ride height of 0.020 m (xz – plane, k – ω SST turbulence model).

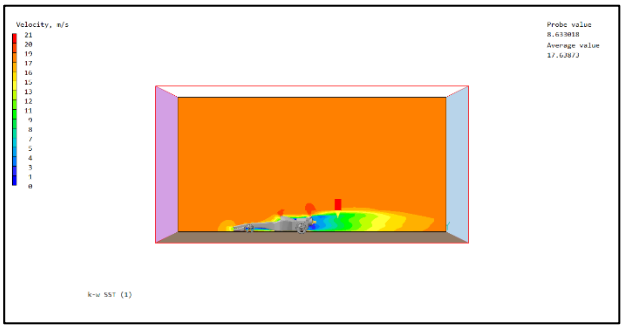

Figure 16: Depiction of the velocity contours, for a ride height of 0.005 m (xz – plane, k – ω SST turbulence model).

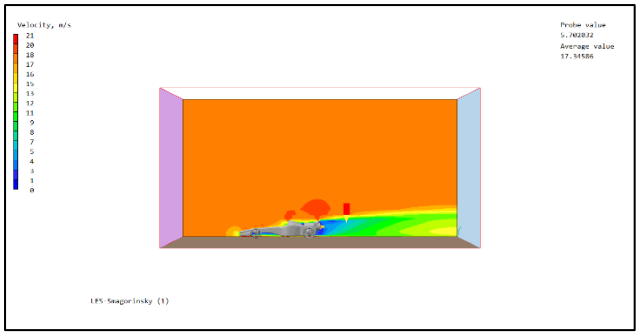

Figure 17: Depiction of the velocity contours, for a ride height of 0.005 m (xz – plane, LES – Smagorinsky turbulence model).

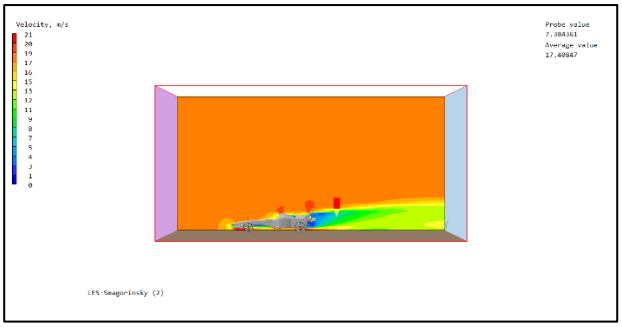

Figure 20: Depiction of the velocity contours, for a ride height of 0.010 m (xz – plane, LES – Smagorinsky turbulence model).

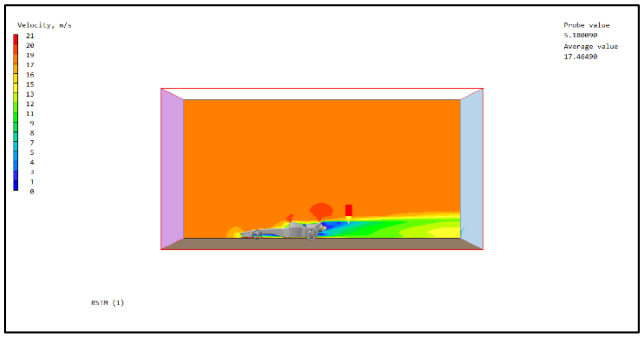

Figure 18: Depiction of the velocity contours, for a ride height of 0.005 m (xz – plane, RSTM).

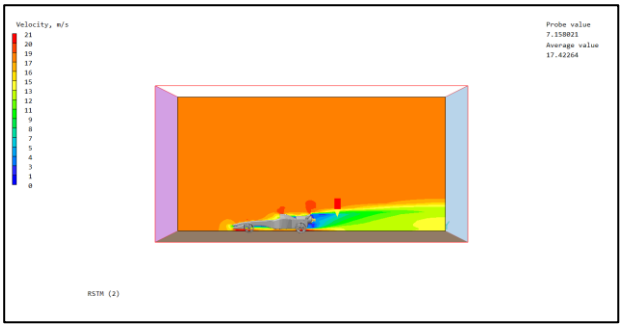

Figure 21: Depiction of the velocity contours, for a ride height of 0.010 m (xz – plane, RSTM).

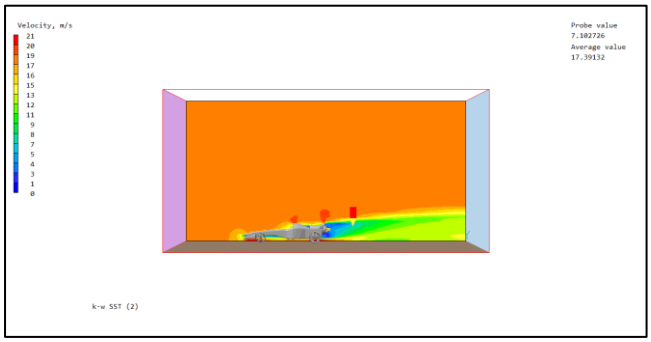

Figure 19: Depiction of the velocity contours, for a ride height of 0.010 m (xz – plane, k – ω SST turbulence model).

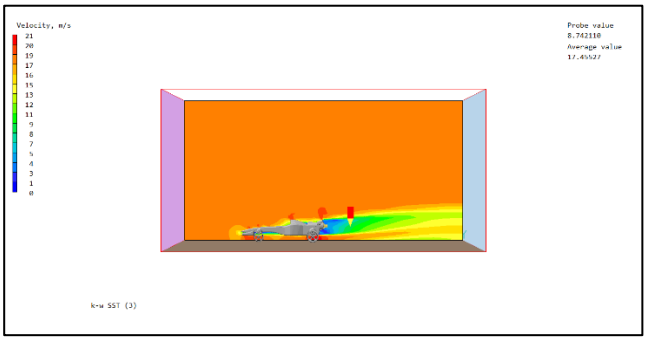

Figure 22: Depiction of the velocity contours, for a ride height of 0.020 m (xz – plane, k – ω SST turbulence model).

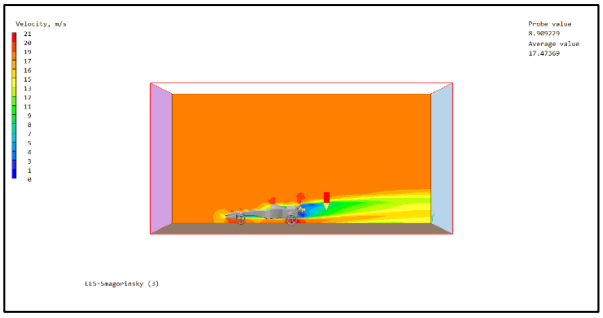

Figure 23: Depiction of the velocity contours, for a ride height of 0.020 m (xz – plane, LES – Smagorinsky turbulence model).

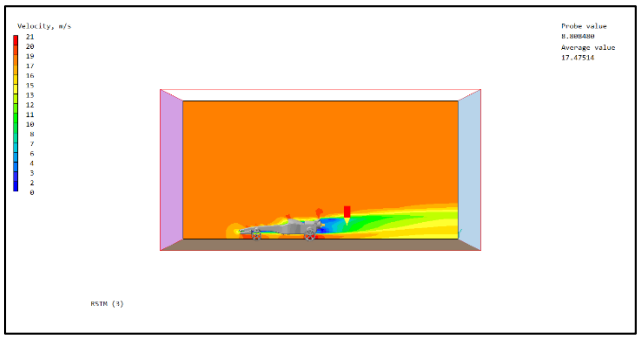

Figure 24: Depiction of the velocity contours, for a ride height of 0.020 m (xz – plane, RSTM).

Inspection of the velocity fields (*Figures 16 – 24*), reveals that the air velocity right behind the vehicle has a very low value, something that is reasonable and expected, due to the car body's interference with the air flow direction.

Furthermore, two areas of increased velocity can be distinguished, mainly on top of the back of the vehicle, and specifically, just above the engine's cover and the rear wing. It is possible that the reason for this is the alteration in the velocity direction at those spots, as it changes from horizontal to slightly diagonal, facing upwards. This fact results in the confluence of those vectors with the, already existing, horizontal vectors above them, leading to the high velocity areas mentioned above.

To make this observation more understandable, the velocity vectors distribution is presented in *Figure 25*, as predicted by the k – ω SST turbulence model, for a ride height of 0.005 m, where this phenomenon is more distinct.

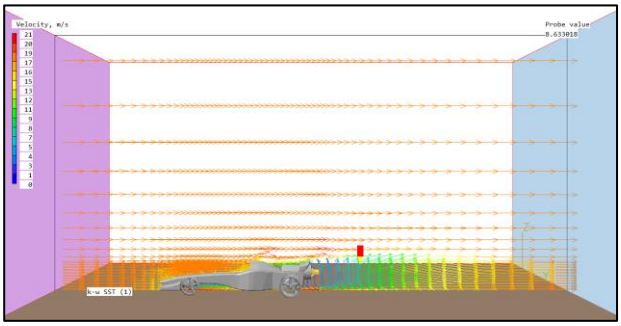

Figure 25: Depiction of the velocity vectors, as predicted by the k – ω SST turbulence model and a ride height of 0.005 m, where the abrupt change in the direction of the vectors, above the engine's cover and the rear wing is clearly visible.

Apart from the aforementioned observations, by examining the pressure distributions (*Figures 7 – 15*), it becomes clear that, just like in the case of the air velocity, there are areas of increased pressure. Those areas are, for the most part, located at the front wing and in front of the engine's cover, which are parts of the car's body, therefore obstacles to the air flow. On the contrary, just behind the vehicle's body and wheels, the pressure has a low value. This is due to the existence of strong flow recirculation, in those areas. These flow recirculations are noticed in the direction of the vectors of the air x – velocity, as can be seen in *Figure 25*.

5.2. Study of the rear wheel diameter's effect

In the second case, changes were made in the rear wheel diameter, and their effect on the flow field and on the drag and lift coefficients was studied.

5.2.1. Geometrical characteristics

In *Table 10*, the geometrical characteristics, for the three cases studied, are shown.

Table 10: The model's dimensions, which were used in the three examined cases (expressed in meters).

Case	Ride height	Front wheel diameter	Rear wheel diameter	Length	Width	Height
4	0.005	0.030	0.031	0.294	0.042	0.054
5	0.005	0.030	0.035	0.294	0.042	0.054
6	0.005	0.030	0.040	0.294	0.042	0.054

In the particular case study, the ride's height was set equal to 0.005 m and remained constant, throughout all the calculations, while the front wheel diameter was set equal to 0.030 m. This is the minimum allowed value by the Formula 1 standards. The rear wheel diameter's value was initially set equal to 0.031 m and then changed to 0.035 m and 0.040 m.

The results obtained for the nine cases performed (3 diameter values times' 3 turbulence models) are presented in the following section.

5.2.2. Results and observations

The results of this study are listed in *Table 11*.

Table 11: Effect of the rear wheels' diameter on the calculated drag and lift coefficients, for the three turbulence models.

Case	Turbulence Model	Rear wheel diameter (m)	Drag Coefficient (C_d)	Lift Coefficient (C_l)
1.4	k – ω SST	0.031	0.626	0.212
1.5	k – ω SST	0.035	0.660	0.146
1.6	k – ω SST	0.040	0.616	0.094
2.4	LES – Smagorinsky	0.031	0.747	0.398
2.5	LES – Smagorinsky	0.035	0.860	0.254
2.6	LES – Smagorinsky	0.040	0.627	0.089
3.4	RSTM	0.031	0.691	0.282
3.5	RSTM	0.035	0.752	0.170
3.6	RSTM	0.040	0.615	0.076

It is observed that, for all three turbulence models, the drag coefficient initially increases significantly with the diameter and, subsequently declines, reaching a value, which is lower than that for the initial diameter. The lift coefficient is high for the smaller diameter and then decreases, as the rear wheel diameter increases. It is also clear that both the drag and lift coefficients have their lowest values for the largest diameter of 0.040 m. This observation applies to all three turbulence models used.

Similarly to the previous case study (analyzed in **Section 5.1**), the Reynolds stress transport model yields the lowest values of drag

and lift coefficients, in comparison with the other two turbulence models.

For a rear wheel diameter of 0.040 m (the diameter, for which the drag and lift coefficient have the lowest values), the drag coefficient calculated using the RSTM is **0.1623%** and **1.914%** lower than the ones calculated, using the k – ω SST and LES – Smagorinsky turbulence models, respectively. Higher differentiation between the calculated values is noticed for the lift coefficient, as it is **19.15%** and **14.61%** lower than the values calculated by the k – ω SST and LES – Smagorinsky turbulence models, respectively.

In *Figures 26 – 43*, pressure and velocity contours, viewed in the xz – plane, for the three different rear wheel diameters and the three different turbulence models, are displayed.

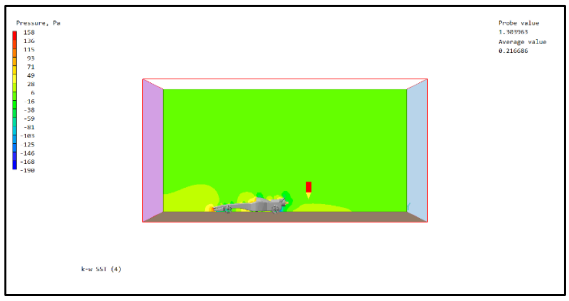

Figure 26: Depiction of the pressure contours, for a rear wheel diameter of 0.031 m (xz – plane, k – ω SST turbulence model).

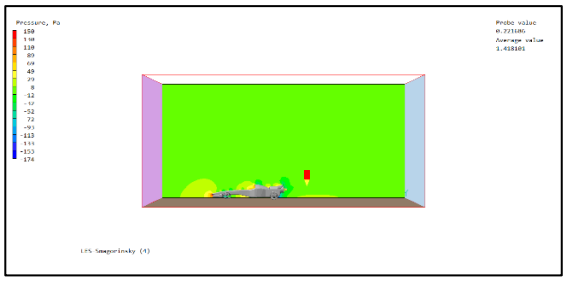

Figure 27: Depiction of the pressure contours, for a rear wheel diameter of 0.031 m (xz – plane, LES – Smagorinsky turbulence model).

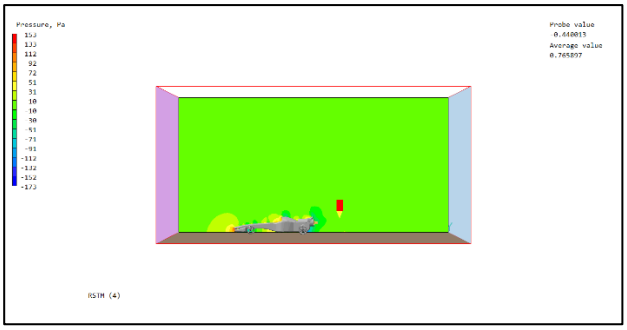

Figure 28: Depiction of the pressure contours, for a rear wheel diameter of 0.031 m (xz – plane, RSTM).

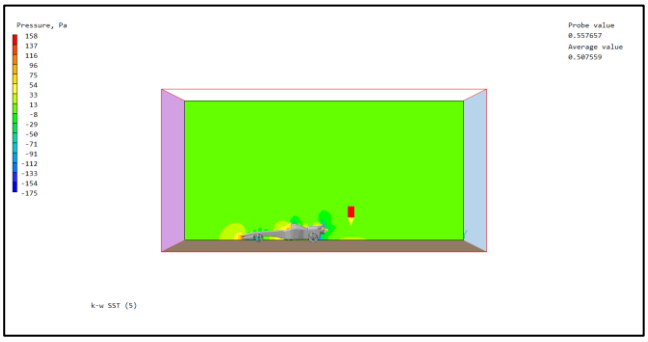

Figure 29: Depiction of the pressure contours, for a rear wheel diameter of 0.035 m (xz – plane, k – ω SST turbulence model).

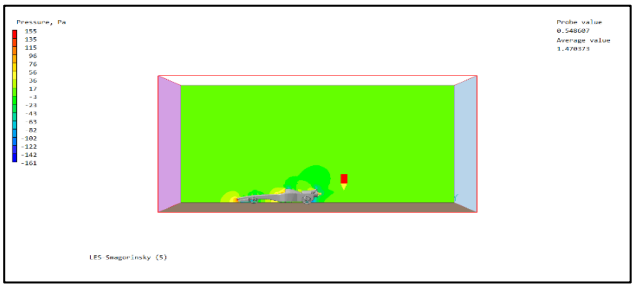

Figure 30: Depiction of the pressure contours, for a rear wheel diameter of 0.035 m (xz – plane, LES – Smagorinsky turbulence model).

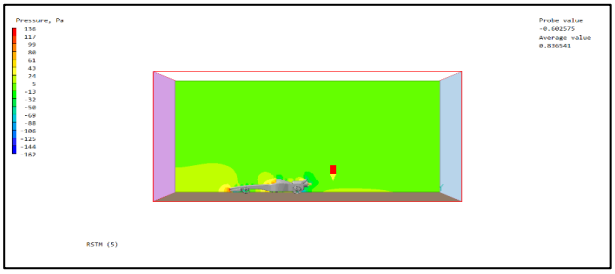

Figure 31: Depiction of the pressure contours, for a rear wheel diameter of 0.035 m (xz – plane, RSTM).

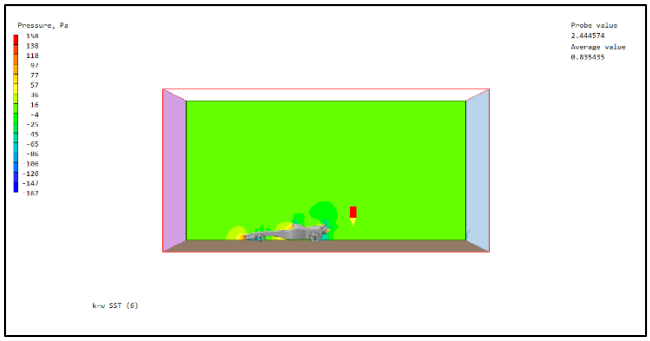

Figure 32: Depiction of the pressure contours, for a rear wheel diameter of 0.040 m (xz – plane, k – ω SST turbulence model).

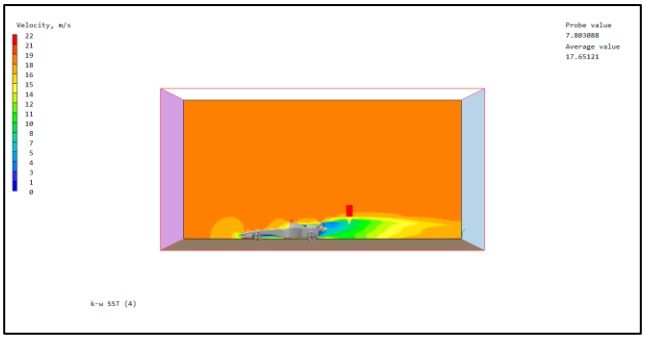

Figure 35: Depiction of the velocity contours, for a rear wheel diameter of 0.031 m (xz – plane, k – ω SST turbulence model).

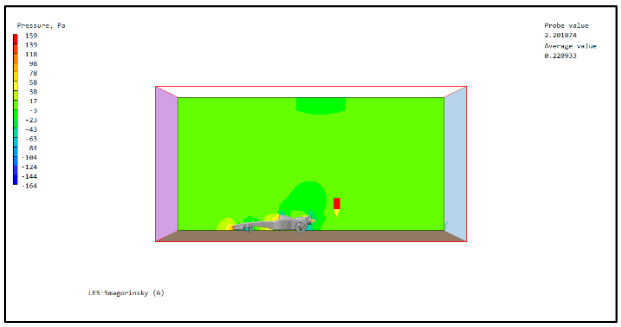

Figure 33: Depiction of the pressure contours, for a rear wheel diameter of 0.040 m (xz – plane, LES – Smagorinsky turbulence model).

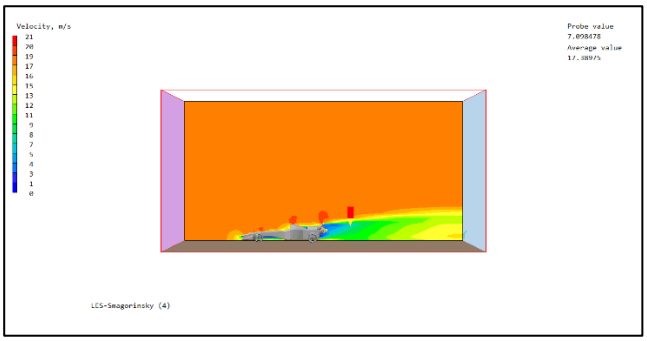

Figure 36: Depiction of the velocity contours, for a rear wheel diameter of 0.031 m (xz – plane, LES – Smagorinsky turbulence model).

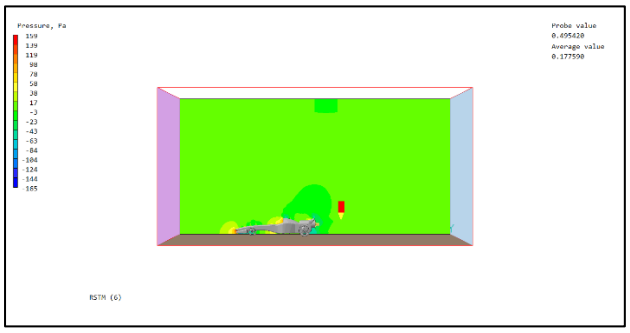

Figure 34: Depiction of the pressure contours, for a rear wheel diameter of 0.040 m (xz – plane, RSTM).

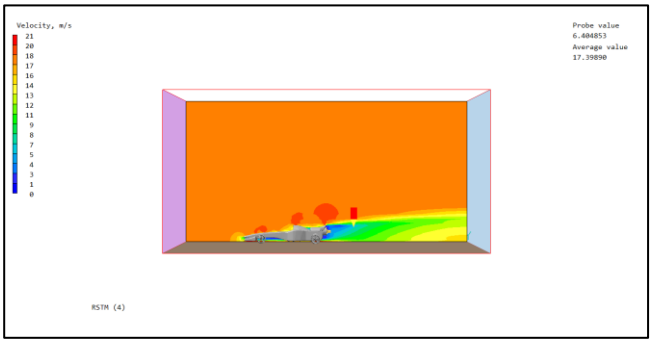

Figure 37: Depiction of the velocity contours, for a rear wheel diameter of 0.031 m (xz – plane, RSTM).

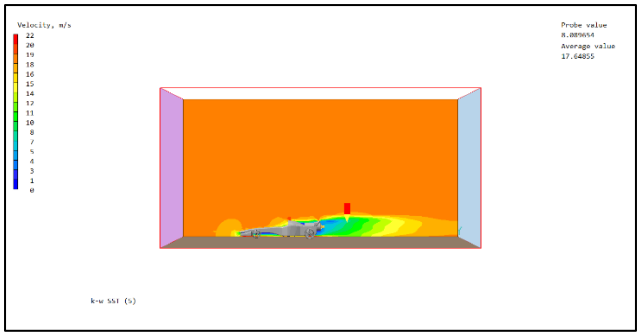

Figure 38: Depiction of the velocity contours, for a rear wheel diameter of 0.035 m (xz – plane, k – ω SST turbulence model).

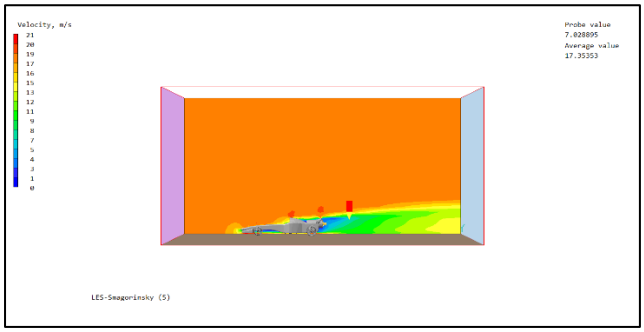

Figure 39: Depiction of the velocity contours, for a rear wheel diameter of 0.035 m (xz – plane, LES – Smagorinsky turbulence model).

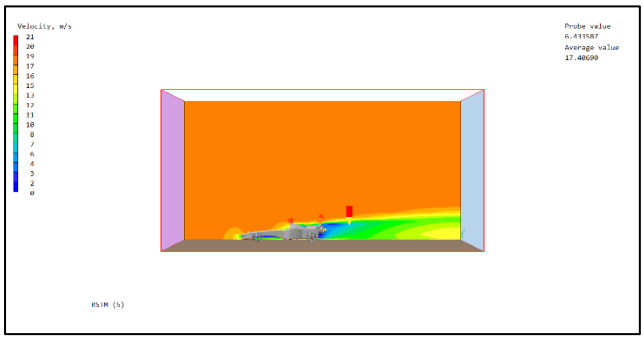

Figure 40: Depiction of the velocity contours, for a rear wheel diameter of 0.035 m (xz – plane, RSTM).

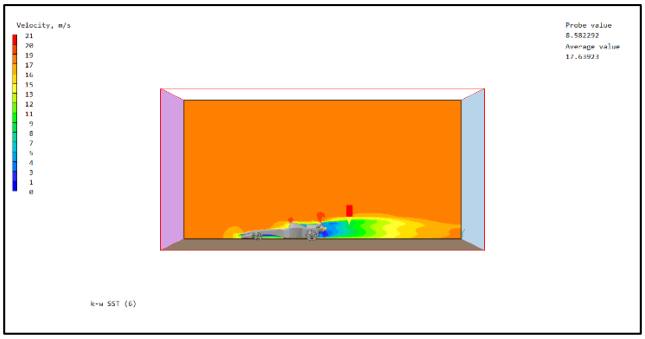

Figure 41: Depiction of the velocity contours, for a rear wheel diameter of 0.040 m (xz – plane, k – ω SST turbulence model).

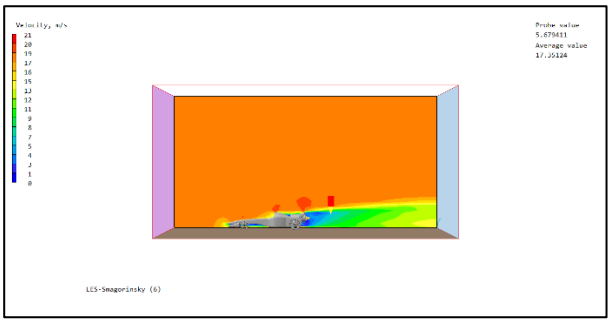

Figure 42: Depiction of the velocity contours, for a rear wheel diameter of 0.040 m (xz – plane, LES – Smagorinsky turbulence model).

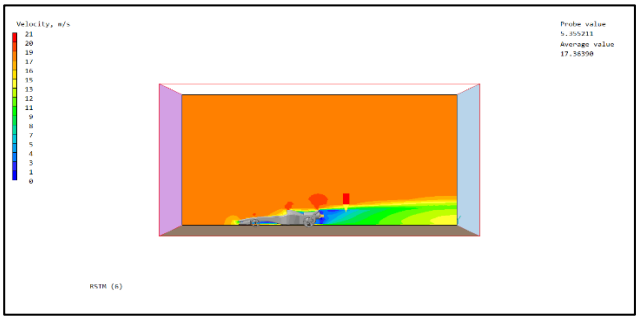

Figure 43: Depiction of the velocity contours, for a rear wheel diameter of 0.040 m (xz – plane, RSTM).

The same observations, about the reduced air velocity, behind the racing car, and the areas of increased velocity, above the engine's cover and the rear wing, which were analyzed in **Section 5.1.2**, apply to this case study as well. Furthermore, there are areas of increased pressure, close to the front wing and the

engine's cover, as well as areas of low pressure, behind the car's body and the car's wheels, due to the, already mentioned, flow recirculations.

6. Comparison with similar studies

The comparison of the present results with the results of similar works [10, 11], reveals that the calculated values of the drag and lift coefficients are located, in most cases, within the same (or at least, similar) range.

More specifically, the first paper [10] refers to the aerodynamic study of a SAE competition Formula 1 vehicle, with the ANSYS Fluent software, by making use of the Langtry – Menter 4 – equation Transitional SST turbulence model [12, 13].

In that study, 3 different vehicle models were analyzed, whereas the air's inlet velocity was considered equal to 25 m/s. Furthermore, the grid's number of elements was approximately equal to 1119641. One of the car models, used in that study, can be seen in *Figure 44*.

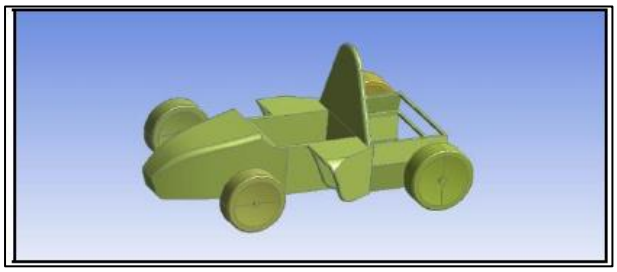

Figure 44: Depiction of the paper's first examined car model [10].

The results obtained for the aerodynamic coefficient values can be seen in *Figures 45 and 46*.

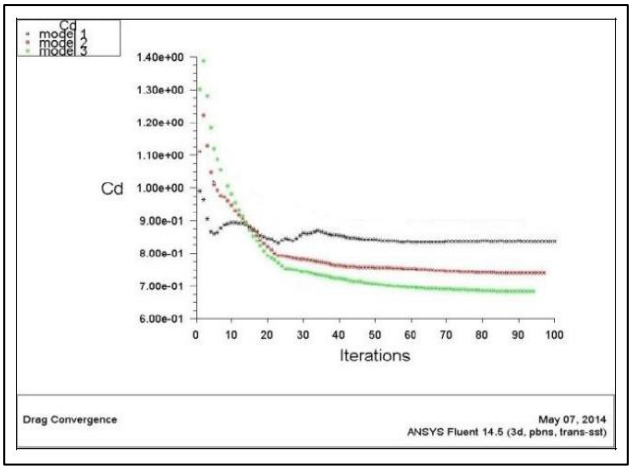

Figure 45: The obtained values of the drag coefficient, for the three different car models [10].

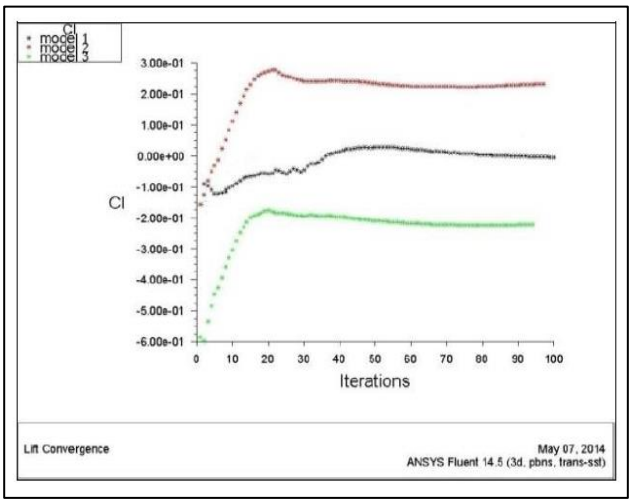

Figure 46: The obtained values of the lift coefficient, for the three different car models [10].

As can be seen in *Figures 45 and 46*, (excluding the values for low iteration numbers, which are less reliable) the results for the drag coefficient's values range from approximately 0.690 to approximately 0.900, while, for the lift coefficient, they range from approximately -0.240 to 0.280, for the different cases studied. Those results are, for the most part, in accordance with the values calculated in the present paper.

The second project [11] is related to the aerodynamic study of a Formula 1 vehicle, created by Brigham Young University, in collaboration with other 26 universities worldwide, with the STAR – CCM+ software, and using the Realizable k – ε turbulence model [14]. The model's geometry can be seen in *Figure 47*.

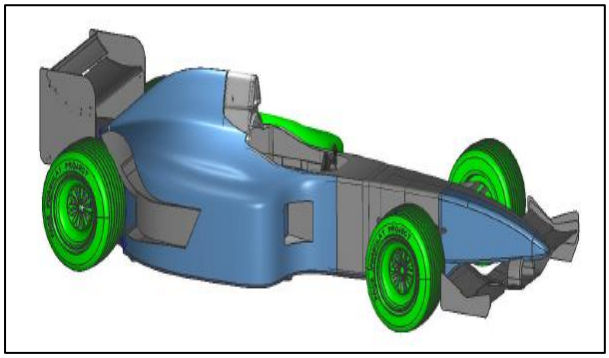

Figure 47: Depiction of the geometry used in the second project [11].

The drag coefficient values, in this case, vary between the values 0.750 and 0.830. Only the values calculated for the two first cases of the case study analyzed in **Section 5.2** of the present paper, and using the LES – Smagorinsky turbulence model, are located within this range or satisfactorily close to it. As for the results acquired, using finer computational grids (see **Section 4**), those regarding the first case study, and especially using the LES – Smagorinsky turbulence model, are similar to those of that project.

The discrepancies observed between the present results and the similar studies in literature are acceptable, in the sense that they are obviously due to the geometrical differences among the different model cars used for the simulations. It is satisfying that all results are in the same overall range and are as physically expected.

7. Conclusions

In the present study, the aerodynamic study of the flow around a Jaguar Formula 1 racing car, was conducted. More specifically, calculations of the aerodynamic drag and lift coefficients, for different cases, and using different turbulence models, took place.

From all the calculations, it became clear that, both the vehicle's aerodynamic characteristics, and the turbulence model, which is used in each case, have a highly significant role in the obtained results. Therefore, even a slight alteration in these settings it is possible to induce a great change in the calculated coefficients' values.

Knowing that the usual value of the drag coefficient, for Formula 1 vehicles, typically ranges between **0.7** and **1.0**, it becomes clear that the results of the simulations of this project are logical and physically correct.

In fact, by observing the results acquired, for the different cases of geometrical characteristics (seen in *Tables 9* and *11*), it is obvious that the values calculated by all models are located satisfactorily close to that range, with those of the LES – Smaroginsky turbulence model, being, in most cases, more precise, than the ones calculated by the k – ω SST turbulence model and the RSTM.

As for the lift coefficient, lower values are desired, thus, it is safe to conclude that the values calculated using the finest grid, are low enough to be realistic.

In conclusion, the existence of divergence between the results of different works is expected, because different geometry, turbulence models and software are used for the calculations, by each one of them. However, our study has managed to maintain a significant level of accordance with similar, already existing studies, as well as with the aerodynamic coefficient values, which are

widely known or found in the scientific literature. The original aspect of this work is that, to the authors' best knowledge, it is the first time that various turbulence models were used for Formula 1 car aerodynamics and proved that such work should be done only using LES, if we want to obtain reliable results, of practical importance.

Acknowledgements

The authors wish to thank CHAM Ltd., London, for allowing them to use their software PHOENICS for performing this work and also the geometry of the Jaguar Model.

References

[1] Almgren, A. S., Bell, J. B., Rendleman, C. A., and Zingale, M. (2006). Low Mach number modeling of type Ia supernovae. I. Hydrodynamics. *Astrophysical Journal* (Vol. 637, pp. 922 – 936).

[2] Hirsch, C. (2007). *Numerical Computation of Internal and External Flows: The Fundamentals of Computational Fluid Dynamics.* Elsevier.

[3] Fielding, S. (2019). *The basics of fluid dynamics.* Durham University.

[4] Argyropoulos, C. D., and Markatos, N.C. (2015). Recent advances on the numerical modelling of turbulent flows. *Applied Mathematical Modelling* (Vol. 39, pp. 693 – 732). Elsevier.

[5] Wilcox, D. C. (2008). Formulation of the k – ω Turbulence Model Revisited. *AIAA Journal* (Vol. 46, pp. 2823 – 2838). AIAA.

[6] Versteeg, H., and Malalasekera, W. (2007). *An Introduction to Computational Fluid Dynamics: The Finite Volume Method (2nd Edition)*. Pearson Education Limited.

[7] Menter, F. R. (1993). Zonal Two Equation k – ω Turbulence Models for Aerodynamic Flows. *AIAA Paper 93 – 2906.* Orlando, FL: AIAA.

[8] Menter, F. R. (1994). Two – equation eddy – viscosity turbulence models for engineering applications. *AIAA Journal* (Vol. 32, pp. 1598 – 1605). AIAA.

[9] Tharwat, R. El – Samanoudy, M., and El – Baz, A. M. R. (2016). Considerations of Stress Limiter for the SST Turbulence Model in Dual Throat Nozzle Predictions. *International Conference on Computational Fluid Dynamics ICCFD9 – 2016 – 123.*

[10] Hetawal, S., Gophane, M., Ajay, B. K., and Mukkamala, Y. (2014). Aerodynamic Study of Formula SAE Car. *Procedia Engineering* (Vol. 97, pp. 1198 – 1207). Elsevier.

[11] Chandra, S., Lee, A., Gorrell, S., and Jensen, C. G. (2011). CFD Analysis of PACE Formula – 1 Car. *Computer – Aided Design and Applications* (Vol. 1, pp. 1 – 14). CAD Solutions, LLC.

[12] Langtry, R. B., and Menter, F. R. (2009). Correlation – Based Transition Modeling for Unstructured Parallelized Computational Fluid Dynamics Codes. *AIAA Journal* (Vol. 47, pp. 2894 – 2906). AIAA.

[13] Menter, F. R., Langtry, R. B., and Völker, S. (2006). Transition Modelling for General Purpose CFD Codes. *Flow, Turbulence and Combustion* (Vol. 77, pp. 277 – 303). Springer.

[14] Shih, T. H., Liou, W. W., Shabbir, A., Yang, Z., and Zhu, J. (1995). A New k – ε Eddy – Viscosity Model for High Reynolds Number Turbulent Flows – Model Development and Validation. *Computers & Fluids* (Vol. 24, pp. 227 – 238). Elsevier.